Minerals Engineering 117 (2018) 14–23

Contents lists available at ScienceDirect

Minerals Engineering

journal homepage: www.elsevier.com/locate/mineng

Numerical simulation of cation exchange in fine-coarse seawater slurry pipeline flow

Cristian Reyes, Christian F. Ihle*

Laboratory for Rheology and Fluid Dynamics, Department of Mining Engineering, Universidad de Chile, Beauchef 850, Santiago, Chile
Advanced Mining Technology Center, Universidad de Chile, Tupper 2007, Santiago, Chile

ARTICLE INFO

Keywords:
Tailings
Cation exchange
Slurry pipelines
CEC
Seawater

ABSTRACT

Slurry pipelines transporting a coarse—the comminution product—and a fine fraction, both in the presence of seawater, can cause an alteration of the liquid phase chemical composition. In the present paper, we present the result of two-dimensional numerical simulations using a mixture model using the OpenFOAM library solving the momentum equations for both the coarse and fine species, the liquid phase, mass transport equations for three ionic species (Ca^{2+}, Na^{+} and Mg^{2+}) and the mean flow continuity. The flow is assumed turbulent, and to this purpose, the k-ϵ model is used. The mass transport has been modeled using a two-species first order kinetic model derived from the Gaines-Thomas exchange equation, assuming the relation between the rate of Ca^{+2}–Na^{+} and that between Na^{+2}–Mg^{+2}. The presence of an inhomogeneous concentration distribution in the vertical and the fine fraction vertical mobility via settling, reveals a strongly inhomogeneous mass transfer characteristic within the pipe section. In particular, the higher particle concentration near the bottom along with lower local velocities of the continuous phase compared to the mid-section imply larger residence times, as confirmed by the numerical results. Both aspects in combination, promote higher Ca^{2+}–Na^{+} and Mg^{2+}–Na^{+} exchange rates near the bottom than in the axis of the pipe. This observation suggests that particle flow heterogeneity may promote or hinder adsorption-desorption processes when compared to homogeneous slurry flows. Results also reveal the potential for the control of the electrolyte structure given the cation exchange capacity (CEC), type and concentration of clays and coarse phase concentration, the latter conditioning the flow structure.

1. Introduction

In the mining industry, transport systems of slurry and water are of primary importance since there are many unit operations that rely on them, especially in mineral processing plants. Pipelines are a common system used in mineral processing because it is extremely flexible and is used in short or long distance for concentrate and tailings. These mixtures contain solid particles that, depending on various aspects, can behave as an equivalent homogeneous fluid or a heterogeneous mixture due to the formation of a bed particles in the bottom of pipe, bringing a non-uniform distribution of particles (Jacobs, 2003; Wilson et al., 2006; Shook and Roco, 2015). Such solid content has a specific size distribution where coarse particles might alter the motion of the fine particles and the liquid phase in the pipe. It is known that when particles are close to the colloidal size, surface forces begin to affect the behavior of the particles in the fluid (Rhodes and Ebrary, 2008).

The presence of clays has various implications in the process. In particular, it affects the pump efficiency in the transport of pulp due its fine size and capacity to change the pulp rheology (Nguyen and Boger, 1998; Ndlovu et al., 2013). On the other hand, it alters the froth stability and surface chemistry of particles in flotation, thus modifying the mineral recovery (Bulatovic, 2007; Farrokhpay and Bradshaw, 2012; Peng and Zhao, 2011). Downstream the process, clays may impact the level of separation of solid from liquid in thickeners *via* the yield stress and the settling characteristics of particles and flocs (Ndlovu et al., 2011; Au and Leong, 2013). In most of the cases, the behavior of clay depends on the electrolyte where it is immersed. In fact, the presence of ions at certain pH develop different process such as sorption, ion exchange and precipitation in the clay surface. In particular, there are many studies that describe the adsorption of heavy metals on clays (*e.g.* Kraepiel et al., 1999; Al-Qunaibit et al., 2005) and some that describe the ion exchange with major cations (Atesok et al., 1988; Carroll and Starkey, 1958). In general, clays interact with cations because the surface charge or zeta potential is a negative product of the isomorphic substitutions of cations of a lower valence. For instance, in the case of montomorillonite, some Al^{+3} are substituted by Mg^{+2} or Fe^{+2}, whereas Si^{+4} are substituted by Al^{+3} (Zarzycki et al., 2007). Thus, cations are adsorbed on the particle surface or exchanged with another

* Corresponding author at: Laboratory for Rheology and Fluid Dynamics, Department of Mining Engineering, Universidad de Chile, Beauchef 850, Santiago, Chile.
E-mail address: cihle@ing.uchile.cl (C.F. Ihle).

https://doi.org/10.1016/j.mineng.2017.12.003
Received 5 August 2017; Received in revised form 22 November 2017; Accepted 3 December 2017
Available online 08 December 2017
0892-6875/

ion to compensate the surface charge. Taking advantage of this feature, clays are used for cleaning wastewater and are considered complex minerals provided that changes in the particle surface can cause changes in the hydrodynamics, rheology, flocculation and sedimentation stability (Zhou et al., 2001; Boger, 2009; Zhang and Peng, 2015).

When modeling the competitive sorption of major cations a common approach is the definition of cation exchange reactions with constant exchange stoichiometry based on equivalent charges. An example is the Gaines-Thomas relation (Voegelin et al., 2000). In the case of pipe flow, CFD is a valid option for modeling two-phase systems. However, to the knowledge of the authors, there are no studies that treat fine and coarse particles in high Reynolds number flows concurrently with a chemical process such as adsorption or ion exchange that may alter the composition of the liquid phase. In this paper, we treat this topic studying its effects on the ion exchange in terms of the chemical and hydrodynamic properties of the system.

2. Governing equations

2.1. Momentum equations

The suspension is modeled as a continuum with solid velocity, density and volume fraction fields $\mathbf{u}_s$,ρ_s and ϕ_s, respectively, superimposed to the liquid with velocity ($\mathbf{u}_l$), density ρ_l and volume fraction $\phi_l = 1-\phi_s$. The momentum conservation equations are

$$\frac{\partial(\phi_i\rho_i\mathbf{u}_i)}{\partial t} + \nabla\cdot(\phi_i\rho_i\mathbf{u}_i\mathbf{u}_i) + \nabla\cdot(\phi_i\boldsymbol{\tau}_i) = -\phi_i\nabla p + \nabla\cdot(\phi_i p_{s,i}) + \phi_i\rho_i\mathbf{g} + \mathbf{f}_i, \tag{1}$$

where the subindex i stands for solid s or liquid l. The pressure is assumed common to both phases. An additional solid pressure contribution $p_s\phi_s$, which sharply increases around the maximum packing fraction $\phi_{\max}$, is added on the momentum equation for the solid in order to bound the volume fraction of solid ϕ_s below $\phi_{\max}$. This extra pressure term in the liquid equation is zero $p_{s,l} = 0$. It is important to note that the volume fraction of fines, ϕ_f, and salt concentration, $C = \sum_i C_i$, affect the liquid density, resulting in a liquid density $\rho_l = \phi_f\rho_f + \phi_{l,C}\rho_{l,C}$, where ρ_s is the solid density and $\rho_{l,s} = \rho_{l,0}(1 + \alpha C)$ is defined as the salt liquid density with $\rho_{l,0}$ the density of fresh water and α an expansion coefficient. The shear stress tensor for each phase is given by Enwald et al. (1996):

$$\boldsymbol{\tau}_i = \mu_i\left(\frac{\nabla\mathbf{u}_i + (\nabla\mathbf{u}_i)^T}{2} - \frac{2}{3}(\nabla\cdot\mathbf{u}_i)\mathbf{I}\right), \tag{2}$$

where the effective viscosity of the solid μ_s is obtained from the expression for the slurry, $\mu_{\text{mix}} = \phi_s\mu_s + \phi_l\mu_l = \mu_l\left(1 + \frac{\phi_s}{\phi_{\max}}\right)^{-[\eta]\phi_{\max}}$, where $[\eta] = 5/2$ is the intrinsic viscosity of a sphere suspension (e.g. Shook and Roco, 2015). Here, $\mu_l = \mu_{l,0}(1 + [\eta]\phi_f)$ corresponds to the suspension viscosity equation, with $\mu_{l,0}$ the dynamic viscosity of the liquid phase. Both can be revised in Enwald et al. (1996). The volumetric forces between phases, denoted by the last term of the right hand side of (2) are given by $\mathbf{f}_i = \mathbf{f}_D + \mathbf{f}_L + \mathbf{f}_{WL} + \mathbf{f}_{TD}$ (Ekambara et al., 2009 and references therein), where $\mathbf{f}_D$ is the drag force, $\mathbf{f}_L$ is the lift force, $\mathbf{f}_{WL}$ is the lubrication wall force and $\mathbf{f}_{TD}$ is the turbulent dispersion force. Here, $\mathbf{f}_i = \mathbf{f}_s = -\mathbf{f}_l$ is the force per unit volume the fluid applies on the solid. For these interfacial forces, we consider same expressions and parameters used in the non-cohesive three-dimensional slurry flow modeling by Ekambara et al. (2009) using ANSYS-CFX.

2.2. Particle transport equations

The mass transport equation for the solid phase, including fine particles, is:

$$\frac{\partial(\phi_i\rho_s)}{\partial t} + \nabla\cdot(\phi_i\rho_s\mathbf{u}_s) = \kappa\nabla^2\phi_i\rho_s, \tag{3}$$

Here, κ is the mass diffusivity coefficient, and $i = f$ or s. It has been assumed that the clay particles move with the liquid, except on the vertical velocity, where the sedimentation is allowed. This assumption has been proven reasonable in comparison with the full set of coarse and fine equations, and allows saving significant computational times. The fine particle velocity is defined as $\mathbf{u}_{s,f} = -w_{s,f}\hat{\mathbf{k}}$, and corresponds to the Stokes velocity corrected by a hindrance function (Richardson and Zaki, 1954):

$$w_{s,f} = \frac{1}{18}\frac{(\rho_s-\rho_l)d_f^2}{\mu_{l,0}}(1-\phi_T)^{4.65}, \tag{4}$$

where d_f is the fine fraction diameter (the clay fraction) and $\phi_T = \phi_f + \phi_s$ is the total volume fraction of particles.

2.3. Salt transport equations

The salt concentration satisfies the advection-diffusion equation

$$\frac{\partial(\phi_l\rho_l C_i)}{\partial t} + \frac{\mathrm{d}S_i}{\mathrm{d}t} + \nabla\cdot(\phi_l\rho_l C_i\mathbf{u}_l) = D\nabla^2(\phi_l\rho_l C_i), \tag{5}$$

where D is the salt diffusivity coefficient, which is taken as $D = 25\kappa$ (Schulte et al., 2016), i = Na,Mg,Ca or Cl. The term $\mathrm{d}S_i/\mathrm{d}t$ is the source term (in the case of Cl is 0) and refers to the ion exchange of the ion pair within the liquid and the fine solid phase, and is defined as:

$$\frac{\mathrm{d}S_j}{\mathrm{d}t} = w_{m,j}\left(\frac{\partial S_j^*}{\partial t} + \nabla\cdot(S_j^*\mathbf{u}_\mathbf{f})\right) = w_{m,j}(R_{1,j}^* + R_{2,j}^*), \tag{6}$$

where $w_{m,j}$ is a unit conversion factor from mol to grams, is the concentration of the ion j = Mg or Ca in kg/m^3, S_j^* is the ion concentration, in mol/m^3, $R_{1,j}^*$ and $R_{2,j}^*$ are derived from the Gaines-Thomas equilibrium equation for ion exchange (Voegelin et al., 2000). For the case of calcium (or magnesium, replacing Ca by Mg):

$$R_{1,\text{Ca}}^* = -k_1\frac{S_{\text{Ca}}^* z_{\text{Ca}}}{\text{CEC}_c}\left(\frac{a_{s,\text{Na}}}{c_0}\right)^2 \tag{7}$$

$$R_{2,\text{Ca}}^* = k_2\left(\frac{S_{\text{Na}}^* z_{\text{Na}}}{\text{CEC}_c}\right)^2\frac{a_{s,\text{Ca}}}{c_0}, \tag{8}$$

with k_1 and k_2 the kinetic constant, in mol/m^3 s, and z_i is the charge of the ion i. Here, c_0 is a reference unit that equals 1 M (Voegelin et al., 2000). On the other hand, $R_{1,\text{Ca}}^*$ is defined as the rate of exchange of calcium in particles with liquid. It also corresponds to the rate of exchange of sodium in the liquid phase with particles. If $R_{2,\text{Ca}}^*$ is higher than $R_{1,\text{Ca}}^*$, then calcium (or magnesium) can go to the particles. Otherwise, the sodium goes to the particles. In (7) and (8), $a_{s,i} = a_{b,i}\exp\left(\frac{-z_i e\zeta}{k_b T}\right)$, where e is the charge of an electron, ζ is the zeta potential, k_B is the Boltzmann constant, T is the absolute temperature and $a_{b,i} = \gamma_i C_i w_{m,i}$ is the surface ion activity, in mol/m^3. Here, $w_{m,i}$ is the molecular weight and γ_i is the activity coefficient, determined by B-dot Model (Bethke, 2007) as:

$$\log\gamma_i = -\mathscr{A}z_i^2\left(\frac{\sqrt{I}}{1 + a_i B_i\sqrt{I}} - \dot{B}_i I\right). \tag{9}$$

Here, $\mathscr{A}$ is a constant, a_i,B_i and $\dot{B}_i$ are ion-dependent constants, and I is the ionic force determined by $I = \sum_i z_i m C_i$ with mC_i the molal concentration of ion i. On the other hand, CEC_c is the calculated cation exchange capacity determined by $\sum z_i S_i$. It is noted that k_1 and k_2 are critical on fixing the timescale of the exchange process. Given a constant mean flow velocity, this implies that the kinetic constant may have a strong relevance on the cation exchange entry length within pipeline (Section 4). For this system, it was assumed that calcium and magnesium ions exchange moles with ion sodium but there is not a

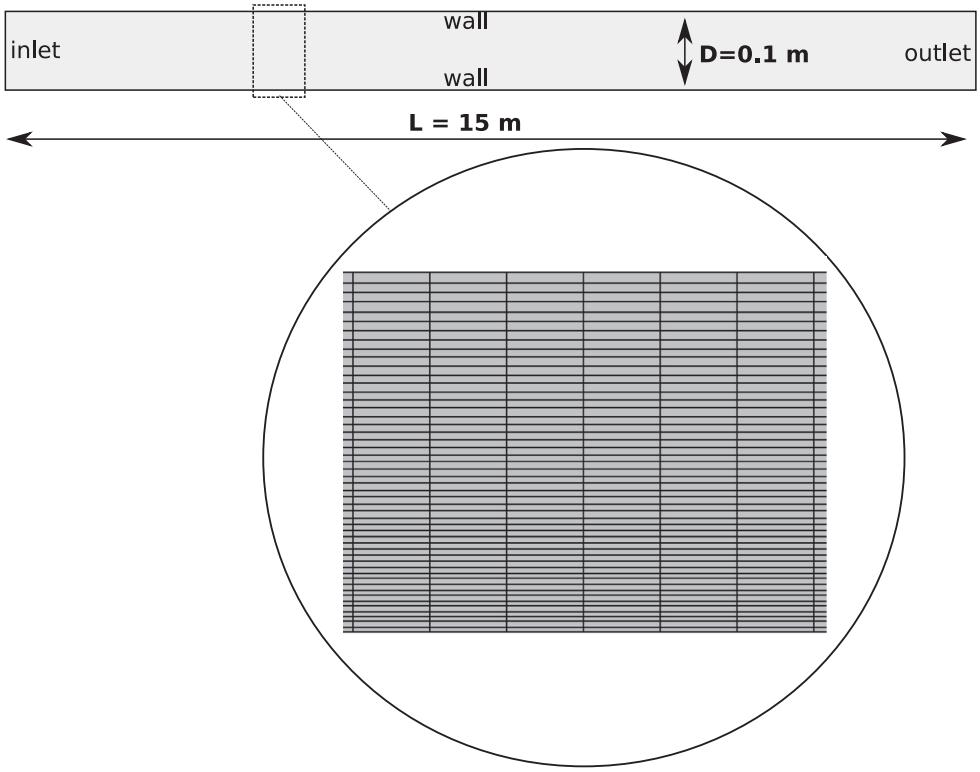

Fig. 1. Schematic of the two-dimensional mesh considered used the simulation, which becomes denser approaching the bottom horizontal wall of the computational domain.

direct exchange between Ca and Mg. The corresponding exchange reactions are given by:

$$2NaX + Ca^{+2} \rightleftarrows 2Na^{+} + CaX_2 \tag{10}$$

$$2NaX + Mg^{+2} \rightleftarrows 2Na^{+} + MgX_2, \tag{11}$$

where X is a negatively (−1) charged site. This allows to calculate the net exchange rate for sodium by stoichiometry as

$$\frac{dS_{Na}}{dt} = 2\left(\frac{dS_{Ca}}{dt} + \frac{dS_{Mg}}{dt}\right), \tag{12}$$

where S_i was defined as, $S_i = \phi_f \rho_f s_i$, with s_i the concentration of the ion i in kg per kg of particle. We assume that initially, the CEC is associated solely to the sodium ions in the fine particles. In practice, often the cation exchange capacity refers to more than one ionic species (Carroll and Starkey, 1958). We, however, consider a single species (as in the homoionic sodium montmorrillonite studied by Tarchitzky et al. (1993)) to simplify the analysis. Therefore, the following relation was $S^*_{Na,0} = \phi_f \rho_f \mathrm{CEC}/100$, with $S^*_{Na,0}$ the initial concentration of the ion Na in the fine particle (clay) in mol/m^3 and CEC the cation exchange capacities of the clay in meq/100 gr clay.

2.4. Turbulence closure

The turbulent model used for the flow of the liquid phase is the two-equation k–ϵ model with standard empirical constants. Using Einstein notation,

$$\frac{\partial}{\partial t}(\rho_l \phi_l k) + \frac{\partial}{\partial x_i}(\rho_l \phi_l u_{l,i} k) = \frac{\partial}{\partial x_i}\left[\rho_l \phi_l \left(\mu + \frac{\mu_{l,\mathrm{turb}}}{\sigma_k}\right)\frac{\partial k}{\partial x_i}\right] + \rho_l \phi_l (G - \epsilon) + S_k \tag{13}$$

$$\frac{\partial}{\partial t}(\rho_l \phi_l \epsilon) + \frac{\partial}{\partial x_i}(\rho_l \phi_l u_{l,i} \epsilon) = \frac{\partial}{\partial x_i}\left[\rho_l \phi_l \left(\mu + \frac{\mu_{l,\mathrm{turb}}}{\sigma_\epsilon}\right)\frac{\partial \epsilon}{\partial x_i}\right] + \rho_l \phi_l \frac{\epsilon}{k}(C_{\epsilon 1} G - C_{\epsilon 2} \epsilon) + S_\epsilon \tag{14}$$

$$\mu_{l,\mathrm{turb}} = \rho_l C_\mu \frac{k^2}{\epsilon} \tag{15}$$

where $u_{l,i}$ is the ith component of the liquid phase velocity vector, and G represents the generation of turbulent kinetic energy due to the mean velocity gradient (Rusche, 2003). For the liquid phase, the k–ϵ model is applied with the standard constants $C_{\epsilon 1} = 1.44, C_{\epsilon 1} = 1.92, C_\mu = 0.09, \sigma_k = 1.0, \sigma_\epsilon = 1.3$ (Rusche, 2003; Versteeg and Malalasekera, 2007). No turbulence model is applied to the solid phase. However, the impact of the disperse phase on the continuous phase is taken into account through the terms S_k and S_ϵ in Eqs. (13) and (14), respectively, whose expressions can be found in Sato and Sekoguchi (1975). The term $\mu_{l,\mathrm{turb}}$ is added to the molecular value, μ_l in (2). For every time step, the final value of $\mathbf{u}_l$ and $\mu_{l,\mathrm{turb}}$ is obtained by iteration.

2.5. Initial and boundary conditions

The corresponding boundary conditions at the top and bottom walls are no ion and solid mass normal gradients, thus precluding mass transfer through the walls. At the inlet, velocities, ion and volume concentration of both phases are uniform. At the outlet, the pressure is specified (atmospheric), whereas for the rest of the variables ion and solid mass horizontal gradients are set as null. At the wall, the liquid and particles velocities were set to zero (no-slip conditions).

2.6. Numerical implementation

The model equations described previously are implemented in the solver twoPhaseEulerFoam of the open source software OpenFOAM. The computational domain consists of a two-dimensional $0.1 \times 15\ \mathrm{m}^2$ domain using a 700×50 node mesh. Fig. 1 shows a schematic, where it is shown that the spatial step is constant in the horizontal direction and finer near the bottom wall in the vertical direction (the bottom element height is 1.38 mm while that at the top is 2.77 mm height). The choice of the number of nodes and the additional refinement at the bottom is the result of mesh convergence mass conservation test.

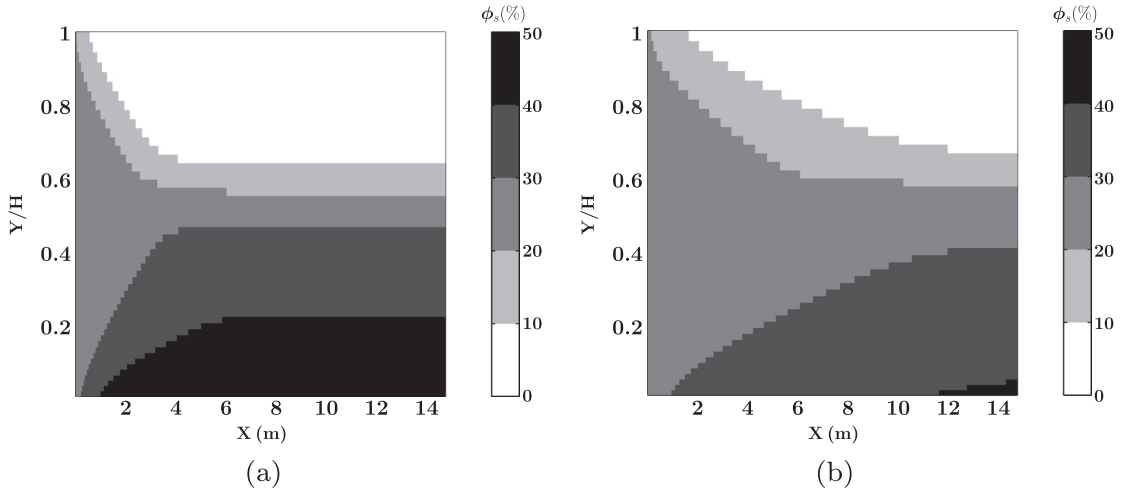

Fig. 2. Coarse particle concentration (ϕ_s) along pipeline with (a) $d_s = 200\,\mu m$ with $u_m = 1\ m\ s^{-1}$ (mean flow velocity), and (b) $d_s = 200\,\mu m$ with $u_m = 3\ m\ s^{-1}$.

Reported measurements have been obtained in steady state (after letting the system evolve until no further changes were noticed), at a distance of 1 m from the outlet boundary of the computational domain. This choice of horizontal location of velocity and concentration profiles corresponds to locally uniform flow, i.e., where no horizontal variations occur at steady state. This is depicted on the concentration profiles of Fig. 2.

To initialize the numerical solution, the average solids volume fraction, ion concentration and a parabolic velocity profile are specified as initial conditions. The initial values of coarse and fine particle volume fractions have been set between 0.2–0.4 and 0.06–0.1, respectively. The values of mean velocities of the liquid and solid phases are 1.0, 2.0 and 3.0 $m\ s^{-1}$ while the adopted values of CEC are 7, 70 and 140. In the liquid phase, the initial concentrations of Na, Ca and Mg are 11.039 g/L, 0.421 g/L and 1.328 g/L, respectively. It has also been considered for the ionic force only (not for the cation exchange process) an initial Cl concentration of 19.85 g/L.

The particle diameter of coarse particles has been set between 10 μm and 200 μm. On the other hand, the fine fraction has been assumed monodisperse, with a diameter equal 1 μm.

Results are obtained from solving for the unknowns $\mathbf{u}_i$ and ϕ_i ($i = s, f$ and l), and C_j (), k and ϵ. With a set of preliminary runs, the present results have been compared with the numerical simulations by Ekambara et al. (2009) and the experimental work by Gillies et al. (2004), with very good agreement, as shown in Fig. 3 for various combinations of particle size, mean flow velocity and solids volume fraction for a monodisperse flow without a cation exchange process. The present output have been found very similar on the vertical velocity and the solid concentration profile to the three-dimensional numerical simulations of Ekambara et al. (2009) and the straight pipe experiments by Gillies et al. (2004), in spite of the fact that present numerical simulations are two-dimensional. The similarity between both is interpreted by the absence of three-dimensional flow features such as secondary currents, caused by anisotropies of normal stresses, which can occur under the presence of singularities such as changes of the flow direction due to bends (Taylor et al., 1982), and departures from circularity of the cross-section of the flow. The latter situation can occur under the presence of a static solid bed in laminar flow. It has been identified that when such normal stress differences are non-negligible, the k-ϵ model is not useful to model secondary currents (Speziale, 1982), and therefore experiments become crucial to identify the extent at which two-dimensional simulations can be reasonably applied.

3. Results and discussion

3.1. Particle distributions and velocity profiles

The overall effect of the presence of a relatively coarse solid phase is to alter the otherwise symmetric velocity profiles with respect to the horizontal centerline. This is explained by the flow heterogeneity where, in zones of higher concentration, causes the mean flow velocity to decrease. This is shown in Fig. 4. For instance, in Fig. 4a (mean flow velocity 2 $m\ s^{-1}$), about 1 mm away from the walls, the velocity in the lower section is about 0.2 $m\ s^{-1}$ lower than that in the upper section. This, on the other hand, corresponds to a solid concentration difference of about 28% between the same sections (Fig. 4b).

Fig. 5 shows the influence of both the mean flow velocity and the mean particle size on the concentration profiles. In particular, Fig. 5a shows that, for a fixed particle size, increasing the particle concentration tends to drive the particle distribution more homogeneous. This is coherent with previous experimental observations (*e.g.* Kaushal et al., 2005), where it is exposed the particle hindrance effect on the settling process within the pipeline. This kind of effect has been also in deposition velocity models (*e.g.* Poloski et al., 2010), where increasing concentration causes a decrease on the deposit velocity. On the other hand, increasing the particle size causes a significant increase on the width of the concentration distribution (Fig. 5b), as expected, and explained by the combined effects of drag and particle (negative) buoyancy.

A different and relevant effect is that of the flow and concentration on the fine particle phase. It is noted, from Eq. (3), that the fine phase local concentration may depart from its initially homogeneous value across the liquid phase if local velocities are small enough to allow for particle settling. A result of the local increase of the coarse particle concentration due to gravity is twofold: first a relatively higher number of coarse particles is related to lower local liquid phase velocities in the interstitial spaces between them, thus potentially enabling for local settling of the fine phase. Second, by virtue of the local continuity of the two-phase mixture, the result of crowding the zone near the bottom with coarse particles is to displace the fluid fraction (plus part of the fine solid phase), to the middle and upper region of the enclosure. This causes an increase of the fine fraction with height, as shown in Fig. 6. This behavior repeats both for different mean flow velocities and bulk concentrations (Fig. 6a and b, respectively).

Fig. 2 shows the nonuniform concentration profile in the flow for the 200 μm coarse particle diameter case, and two very different mean flow velocities ($u_m = 1\ m\ s^{-1}$ and 3 m/s in Fig. 2a and b, respectively). The figure clearly suggests the existence of a particle entry length for

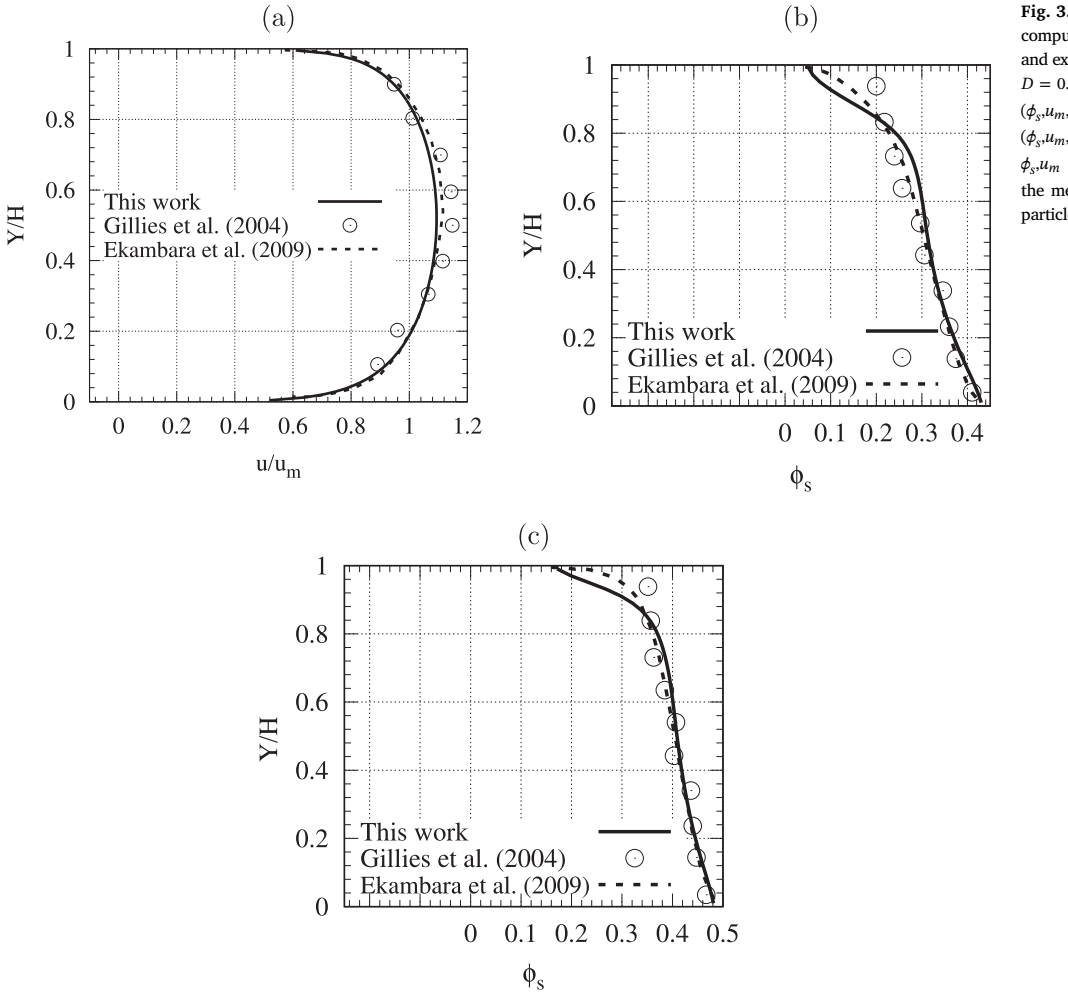

Fig. 3. Comparison between present work with the computational results by Ekambara et al. (2009) and experiments by Gillies et al. (2004), for a height $D = 0.1$ m. (a) $(\phi_s, u_m, d_s) = (0.19, 3\ \text{m/s}, 90\ \mu\text{m})$, (b) $(\phi_s, u_m, d_s) = (0.3, 5.4\ \text{m/s}, 270\ \mu\text{m})$ and (c) $(\phi_s, u_m, d_s) = (0.4, 5.4\ \text{m/s}, 270\ \mu\text{m})$. The symbols ϕ_s, u_m and d_s represent the solid volume fraction, the mean flow velocity and the (monosized) solid particle diameter, respectively.

the coarse mass boundary layer, which depends on the particle size and concentration and the mean flow velocity, where shorter entry lengths are related to higher settling velocities in relation to the mean flow, as depicted on Fig. 2a and b for relatively low and high settling-mean flow velocity contrasts, respectively. This has been reported to some extent by Colwell and Shook (1988) for sand slurries. Although this topic is not pursued further in this paper, for all the cases analyzed, it has been ensured to process within the uniform flow and particle concentration zone.

3.2. Ionic exchange in the system

Fig. 7 shows the result of the cation exchange process for a mean flow velocity (u_m) of $2\,\text{m}\,\text{s}^{-1}$, CEC = 70 meq/100 gr clay, $\phi_s = 20\%$ and $d_s = 100\ \mu\text{m}$, both for the calcium and magnesium. Here, we define the exchanged calcium content in the liquid phase (i.e. outside the clay structure) as

$$\theta_{Ca}(\%) = 100 \times \left(1 - \frac{[Ca^{+2}]}{[Ca^{+2}]_0}\right), \tag{16}$$

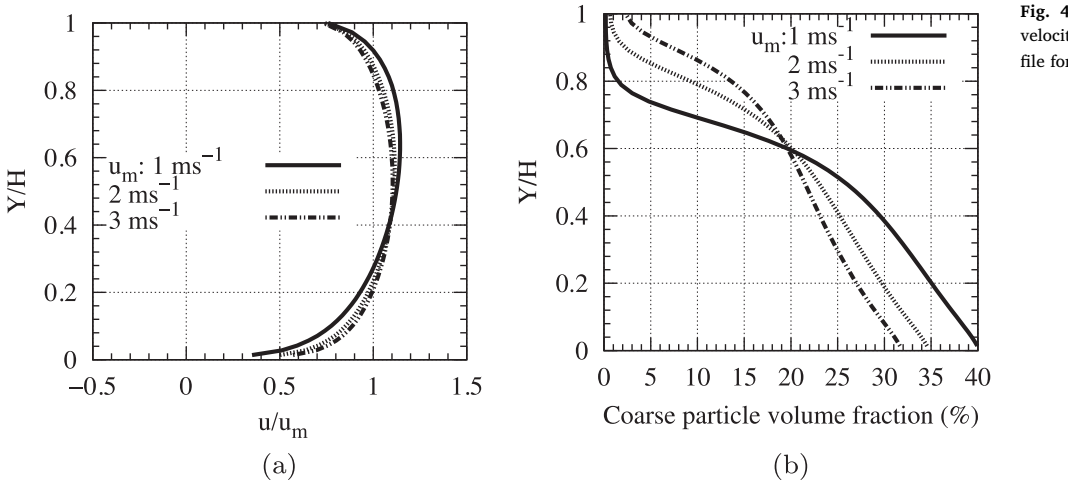

Fig. 4. (a) Velocity profiles for different mean velocities with $\phi_s = 20\%$. (b) Coarse particle profile for different mean velocities.

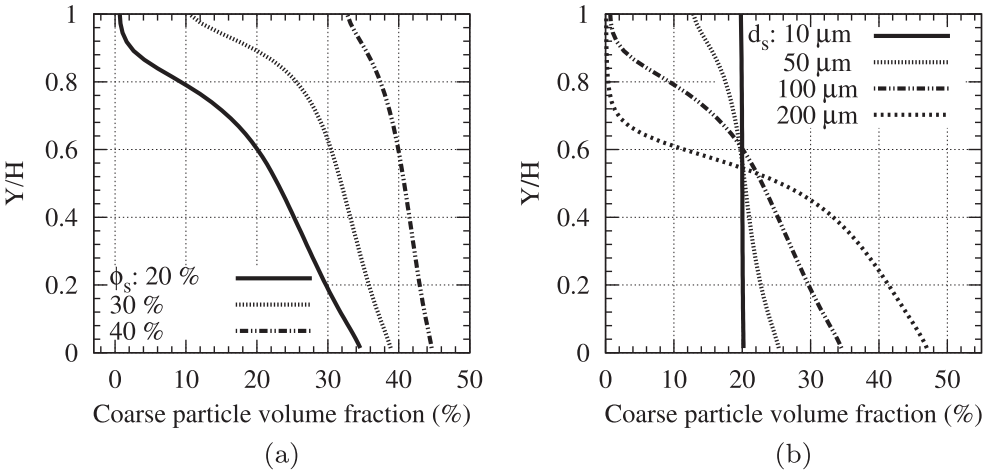

Fig. 5. (a) Coarse particle concentration profiles for different mean coarse concentrations. (b) Particle concentration profiles for different particle sizes. In (a) and (b), the mean flow velocity (u_m) is 2 m s^{-1}.

where the square brackets denote the local, space- and time-dependent molar concentration of calcium in the liquid phase and the subscript 0 corresponds to the (homogeneous) initial value. Here, higher values of θ_{Ca} correspond to higher cation exchange rates between phases. On the other hand, we define $\bar{\theta}_{Ca}$ as the vertical mean exchanged fraction in a cross-section of a pipe. Except for the study of convergence into the pipeline, this mean value was calculated at fixed distance equal 14 m from the inlet of the pipe.

The slight differences between Fig. 7a and b are due to the difference between the Mg and Ca kinetic constants. The corresponding selectivity depends on the kind of clay, the cations present in this particle and the ion in solution, as observed in Carroll and Starkey (1958), where magnesium and calcium is exchanged with sodium from seawater, but the level of exchange is function of the clay used, the montmorillonite used in that experiment has a preference for magnesium, even also exchange calcium with magnesium. Generally, the divalent cations have preference above monovalent cations and, on the other hand, Ca^{+2} above Mg^{+2} (Grim, 1968), but this depends on the system conditions such as the ion concentrations of both the liquid and the particle phase. Here, to reproduce this effect on the numerical simulation, we assume $k_{2,Mg} = 0.5k_{2,Ca}$, with $k_{2,i}$ from Eq. (8). A remarkable feature of this process is the correlation between the local coarse particle concentration and the exchanged cation values. It is apparent from present results that lower local flow velocities are related to higher values of the θ_{Ca} parameter (Fig. 7). In particular, higher coarse fractions are related to lower particle interstitial velocities (seen by the top/bottom velocity ration in Fig. 4a), an aspect that promotes higher residence times and thus higher values of θ_{Ca}. On the other hand, the process of particle settling tends to displace the fluid and fine particle phases (fine particles in this case being mostly advected by the liquid phase). The higher particle fractions present in the zone above the high concentration bottom layer cause higher available areas for cation exchange, thus explaining the non-monotonic characteristic of the θ_{Ca}-curve (Fig. 8a).

On the other hand, it is shown that given a constant fine particle concentration, the effect of the coarse particle size on the local values of θ_{Ca} is slight. A closer view of such differences is depicted on Table 1, where for fine concentrations between 6% and 8%, and coarse particle sizes between 10 µm and 200 µm, mean values of θ_{Ca} are below 2.5%.

The chemical property that has a direct impact on cation exchange capacity in the system is naturally the CEC. Different values of the CEC would generate different cation availabilities in the system and therefore differing values of S_i^*, as shown in Eq. (6). Fig. 8b shows the effect of such parameter for various values of the mean fine particle concentration. As expected, higher CEC values are related to higher values of $\bar{\theta}_{Ca}$. On the other hand, the availability of an increased number of particles per unit volume increases cation exchange values. This is depicted on Fig. 8b.

By virtue of the mass balance in the pipeline, $G_s = \rho_s \phi_T u_m A$ with G_s the throughput, A the cross-sectional area of the pipe, u_m is the mean flow velocity and $\phi_T = \phi_s + \phi_f$. For a fixed value of the throughput and cross-sectional area, Fig. 9a shows that the exchanged fraction of calcium and magnesium decreases as the velocity increases for a fixed value of ϕ_s. In contrast, Fig. 9b reveals that there is a significant increase on $\bar{\theta}_{Ca}$ for modest fine particle fractions, and a tendency to saturation for fine-coarse volume fraction ratios on the order of 100% ($\phi_f/\phi_s \approx 1$). The cation exchange process is thus stimulated by lower flow velocities,

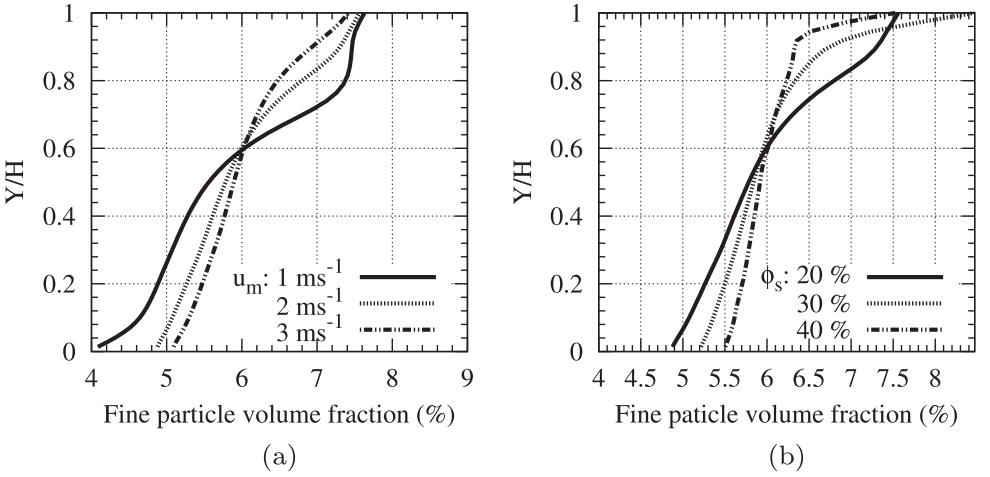

Fig. 6. Fine particle concentration profile for (a) different velocities with ϕ_s = 20% and (b) different coarse particle concentrations. The mean flow velocity (u_m) is 2 m s^{-1} and ϕ_f = 6%.

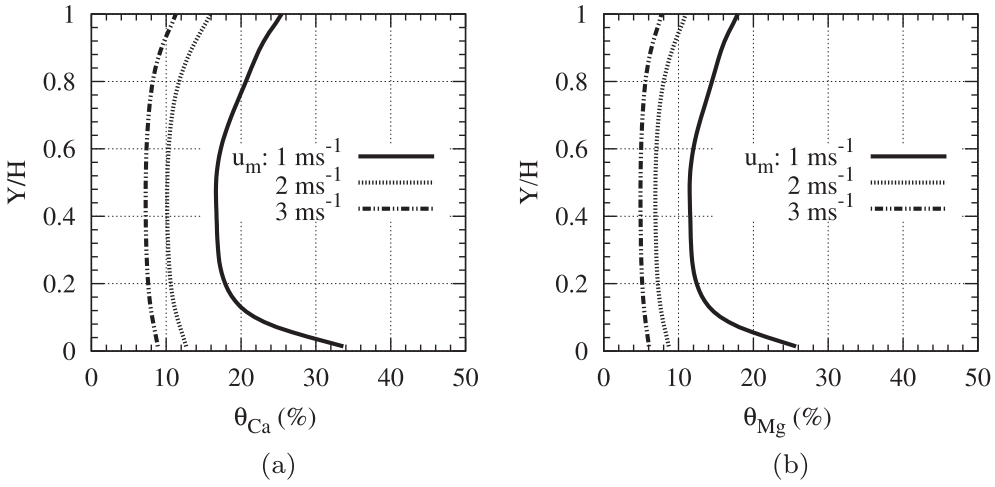

Fig. 7. Cation exchanged fraction in water profiles for (a) calcium y (b) magnesium. Here, $\phi_s = 20\%$,$u_m = 2\,\mathrm{m\,s^{-1}}$, and CEC = 70 meq/100 gr clay.

implying higher residence times and by a higher availability of fine particle fraction in the stream. The nonlinearity of such processes come partially from the nonlinear sorting of fines with mean flow velocity. In this context, when expansive hydrophilic clays are present in the system, fixing the throughput also implies lesser water recovery due to higher water retention in the clays for smaller mean flow velocities or higher fine particle concentrations.

3.3. Affinity of the sodium in the clay

Similarly to the Gaines-Thomas relation, we define the dimensionless constant $K = k_1/k_2$. In chemical terms, this refers to the affinity of sodium with the clay. In equilibrium conditions, where $\mathrm{d}S/\mathrm{d}t = 0$, from (6)–(8),

$$\frac{k_1}{k_2} = \frac{c_0}{\mathrm{CEC}_c}\left(\frac{S^*_{\mathrm{Na}} z_{\mathrm{Na}}}{a_{s,\mathrm{Na}}}\right)^2 \frac{a_{s,\mathrm{Ca}}}{S^*_{\mathrm{Ca}} z_{\mathrm{Ca}}} \tag{17}$$

Fig. 10a, corresponds to the case of a sodium montmorillonite or sodium bentonite, where all the ions available for exchanging are Na^+. Considering a fixed pipeline length, zeta potential and ion concentration in the liquid phase, that the higher the value of k_2, the higher is the exchanged calcium fraction. Also, it is shown that for K = 10,15 and 20, there is a value of k_2 above which the exchanged fraction converges, thus achieving an equilibrium condition in the pipeline. It is also evident from such figure that the lower the value of K, the higher the maximum value of $\bar{\theta}_{\mathrm{Ca}}$. Such value depends on k_2, which is defined in Eq. (8) as the rate than Ca is exchanged with Na from liquid. On the other hand, for $K = 5$, the curve is monotonically increasing in the k_2 range computed. This is because for low values of K, the affinity with Na is low and the clay prefers to keep exchanging sodium with calcium. On the other hand, when $K \leqslant 5$, for fixed values of k_2, more time is required to complete the exchange process and thus to reach the equilibrium condition. In this case, such time is on the order of that required to travel through the pipe length considered in the present numerical simulations, $\tau_L \sim L/u_m$, with L the pipe length and u_m the pulp velocity. Decreasing K for fixed values of k_2 is equivalent to cause a decrease on k_1 which, from (7), cause a decrease on $R^*_{1,Ca}$. For sodium (Fig. 10b) the curve is similar but it is in the another direction, a result of the incorporation of sodium in the liquid phase.

In the case of magnesium (Fig. 10c) trends are roughly the same. However, a comparison of values of $\bar{\theta}_{\mathrm{Ca}}$ and $\bar{\theta}_{\mathrm{Mg}}$ at equal values of k_2 reveals some differences, which are explained due to the differences in

Table 1
Coarse particle diameter d_s effect on calcium mean exchanged fraction.

	$\bar{\theta}_{\mathrm{Ca}}$		
–	ϕ_f(%)		
d_s (μm)	6	8	10
10	11.38	18.87	27.28
50	11.40	18.89	27.29
100	11.38	18.80	27.21
200	11.18	18.50	26.74

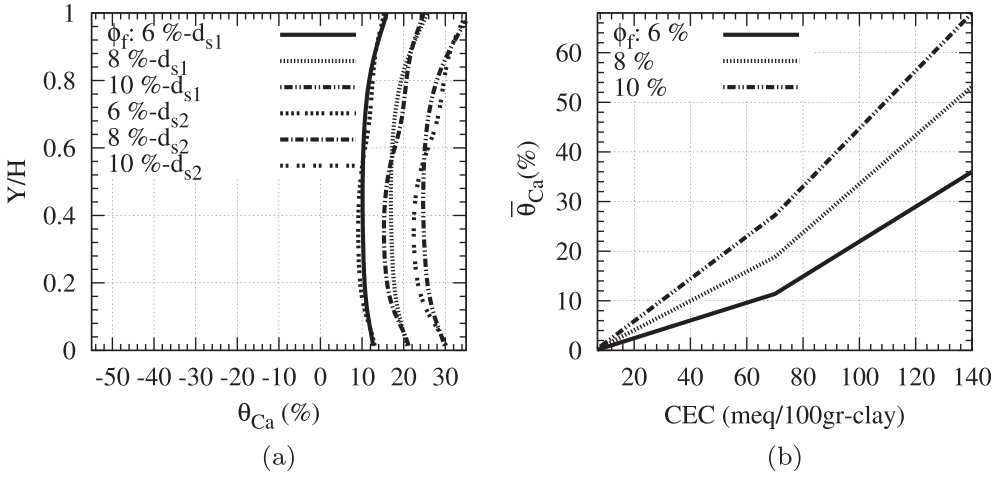

Fig. 8. Calcium exchanged fraction profiles for (a) different clay fractions (d_{s1} = 100 μm,d_{s2} = 200 μm and CEC = 70 meq/100 gr clay) and (b) cation exchange capacities for different clay concentrations, with $\phi_s = 20\%$ and $u_m = 2\,\mathrm{m\,s^{-1}}$.

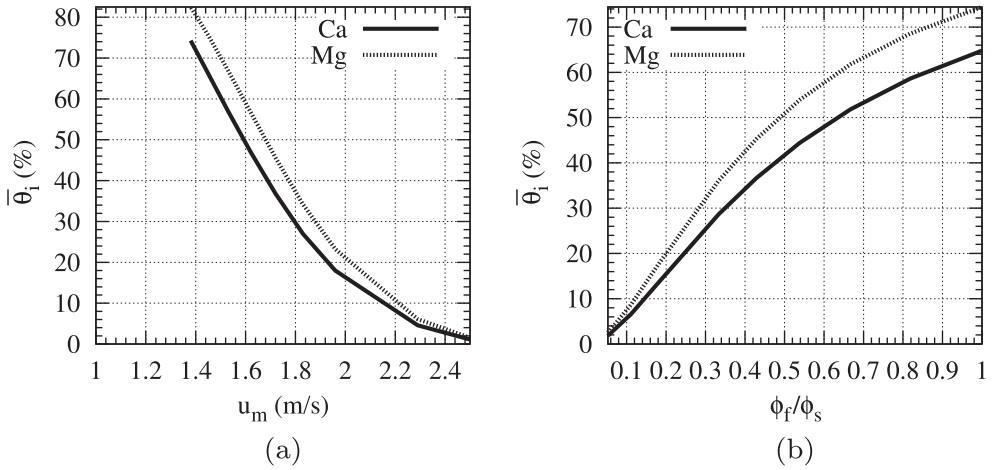

Fig. 9. Mean values for exchanged ion content. (a) In terms of the mean flow velocity, with $\phi_s = 20\%$. (b) In terms of the fine/coarse particle ratio (ϕ_f/ϕ_s), keeping fixed $\phi_T = \phi_f + \phi_s = 40\%$ and $u_m = 2\,\mathrm{m\,s^{-1}}$. In both figures, i = Ca or Mg and CEC = 70 meq/100 gr clay.

initial concentrations and activities ($a_{s,i}$). In both figures, for a slow kinetic (low k_2) the final fraction is similar and they are independent of the affinity with Na because the term R_1^* becomes irrelevant in front of R_2^*. On the another hand, the maximum cation fraction exchanged, θ_{Ca}, for a fixed pipe length is a decreasing function of K. Therefore, this parameter (K) is key to define the capacity of this kind of clay to exchange cations when being mixed with a specific electrolyte.

3.4. Cation competition between Ca and Mg

In addition to the definition of the parameter K, a similar ratio is defined to account for the selectivity of magnesium with respect to calcium: $K_{Mg} = k_{2,Mg}/k_{2,Ca}$. This parameter actually corresponds to an indirect selectivity because it does not consider the reaction between Ca and Mg. Indeed, it reflects a competition between magnesium and calcium through the sodium, on which of both can proceed faster to

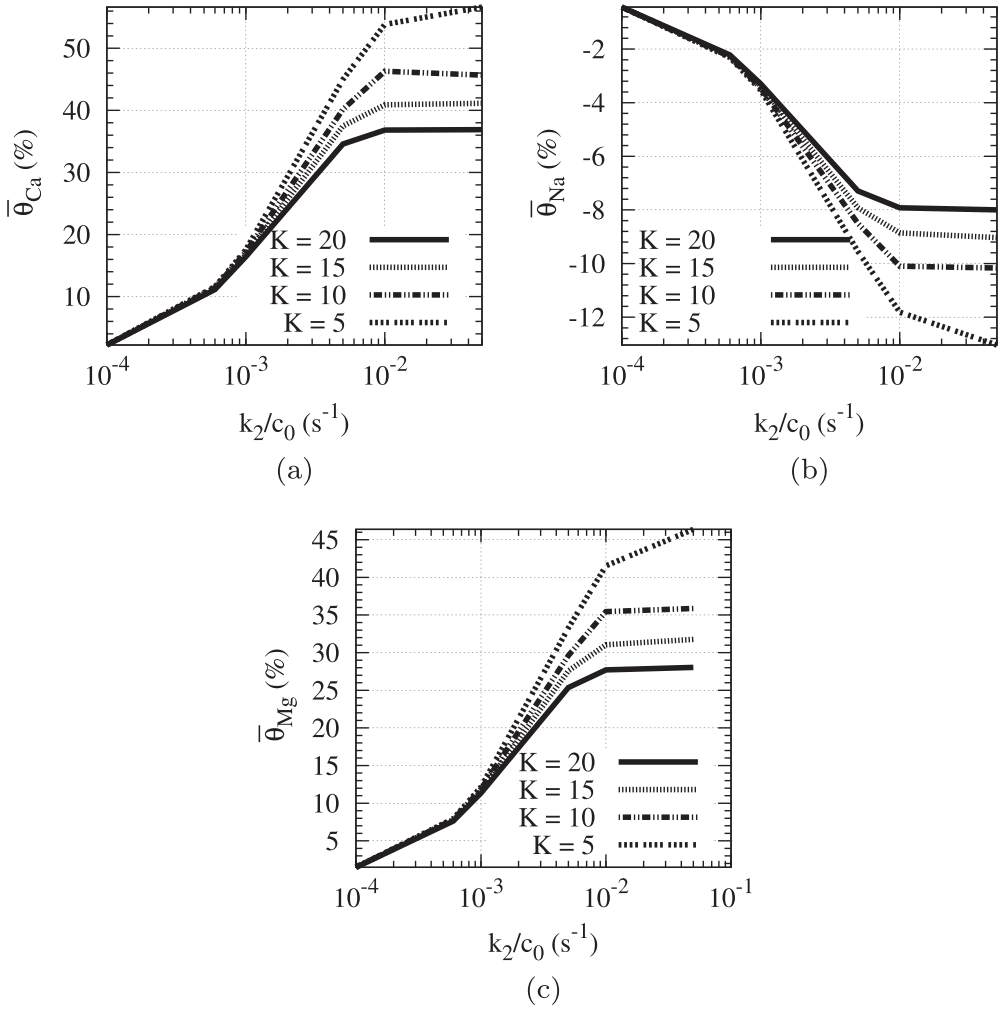

Fig. 10. Mean values for exchanged ion content, as a function of k_2 for different values of K. (a) Calcium, (b) sodium, and (c) magnesium. Here, CEC = 70 meq/100 gr clay, $\phi_s = 20\%$, $\phi_f = 6\%$, $u_m = 2\,\mathrm{m\,s^{-1}}$, and $d_s = 100\,\mu\mathrm{m}$.

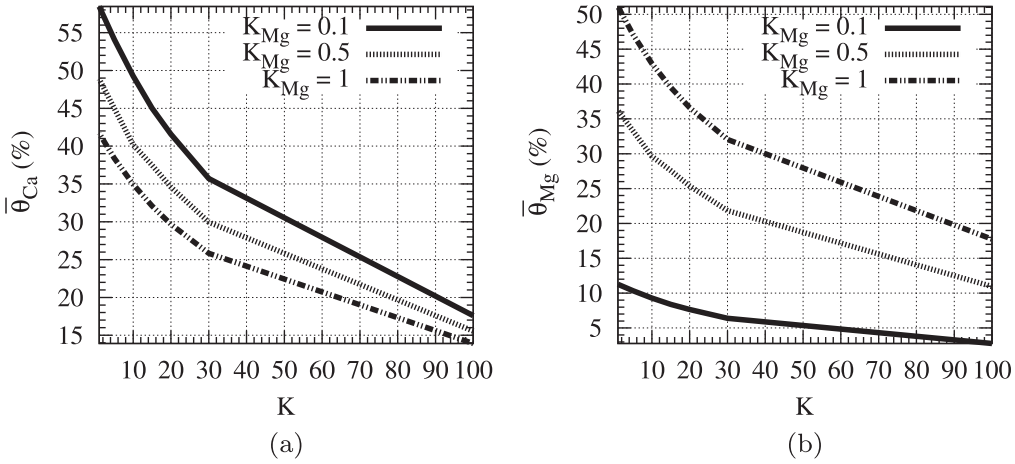

Fig. 11. Effect of K_{Mg} on the exchanged ion fraction for different values of K. (a) Calcium and (b) magnesium. Here, CEC = 70 meq/100 gr clay, ϕ_s = 20%, ϕ_f = 6%, u_m= 2 m s^{-1}, and d_s = 100 μm.

exchange cations with the available sodium in the clay interlayer. For this reason, the higher is K_{Mg}, the lower is the fraction exchanged for Ca because Mg is taking away more Na cations from the interlayer than could have been potentially exchanged with Ca. This effect is stronger in magnesium than calcium as it may be seen in Fig. 11.

4. Cation exchange entry length

Fig. 12 shows that in a high sodium clay, if k_2 is high the convergence will take a shorter length within pipe compared to the low-k_2 case. On the other hand, for a fixed value of K, all the curves converge to the same value but at different distances. This convergence distance is a monotonically decreasing function of k_2, which plausibly depends on the available turbulence for ion transfer towards particles. This sort of flow-dependence has been consistently identified in flocculation, where kinetic constants associated to Brownian and collision-driven flocculation differ by the presence of turbulence (or strong local shearing) in the latter case (Svarovsky, 2000). From the literature, there is no consensus on whether the kinetics of this process are fast or slow. While some authors note than the dynamics are fast (*e.g.* Tang and Sparks, 1993), where the shaken system reaches the equilibrium in 20–60 s, other show, in a static system, and thus in the absence of turbulence, than the equilibrium is reached in a period of days (Karnland et al., 2011). In a mineral processing plant, another important aspect is the impact this cation exchange process causes on pulp critical variables such as rheology (Boger, 2009), flocculation and settling (Concha, 2014), and how does it might contribute to process performance variability. In particular, fluctuations in the zeta potential or internal composition (not addressed herein) may have strong repercussions in the plant results due to change in the interaction with another particles and with chemical reagents. To determine the real value of k_2 and K, could help to define if the clay is susceptible to changes into pipe (or in a reactor) for the ions in liquid. For this system, the equilibrium condition depends on how high are exchange rates, how long is the pipeline or how low is the mean flow velocity, the latter affecting the ion concentration profile and the efficiency of particle transport. This point is critical because it puts together the potential requirement of lower velocities to promote cation exchange and the requirement of sufficiently high flow velocities to ensure particle transport (Abulnaga, 2002).

5. Conclusions

Coarse particle organization in slurry pipelines plays a crucial role on cation exchange processes when a fine fraction is present. In this system, the coarse particle phase causes an influence on the hydrodynamics and eventually on the cation exchange rates into the pipeline. The interplay between the fine fraction and the liquid phase evolves to a physicochemical scenario that can be either beneficial or undesirable in this kind of slurry transport system, which increasingly often mimic those operating in Chilean mineral processing plants. In particular, the cation exchange between sodium and calcium has the potential to reduce the water retention characteristic of the sodium montmorillonite (Abu-Jdayil, 2011), and thus the ability to control the Na^+/Ca^{2+} ratio in

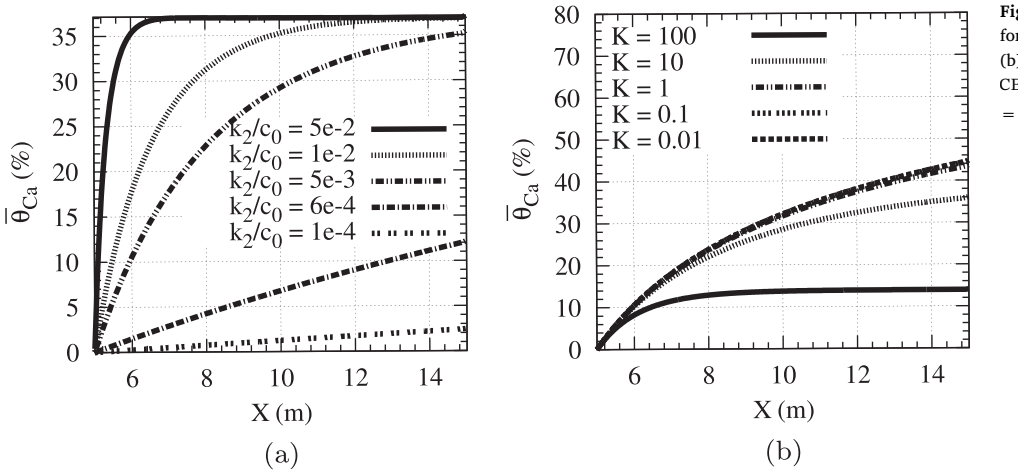

Fig. 12. Exchanged calcium fraction along pipe (X) for (a) different values of the k_2/c_0 ratio (in s^{-1}), and (b) different values of $K = k_1/k_2$. Here, CEC = 70 meq/100 gr clay, ϕ_s = 20%, ϕ_f = 6%, u_m = 2 m s^{-1}, and d_s = 100 μm.

the clay interlayer has an interesting potential.

Present results reveal the existence of a wealth of potential ways to control the ionic content of the water phase, by mixing it with clays with cation exchange properties. In particular, controlling the turbulence into the system, along with the type and amount of fine particles may define the ionic characteristics downstream (*e.g.* in a thickener array or a tailing storage facility), thus conditioning the potential for downstream water recovery or even the onset of reactive flows at tailing deposits or related sites. The present set of numerical simulations reveal that the cation exchange capacity by itself is far from sufficient for an accurate determination of the electrolyte structure. In particular, in the sodium-calcium-magnesium system studied herein, while the affinity of the sodium (present in the liquid phase) through the parameter K, has been assessed in light of a number of hypotheses, yet it is required to study more in detail the interplay between the cations present in the water and those in the clay. In the particular case depicted herein, a specific assumption has been made to expose how is the cation exchange with both calcium and magnesium, where present numerical simulations have been able to predict saturation thresholds for cation exchange both in terms of the fine fraction concentration and the rate at which the cation exchange occurs, given by the parameters k_1 and k_2. The cation selection process from the clay needs a broader analysis, including an experimental validation. Laboratory measurements of cation exchange kinetics would allow for the determination of the corresponding time scales which, *via* the mean flow velocity, are related to a cation exchange entry length. This is being presently studied by the present group of researchers. Fig. 12b gives an illustrative example of the considerable variability that might be found (and is apparent from the diverse results reported in the literature).

On the other hand, a commonly used parameter to assess the cation exchange process is the zeta potential within the suspensions. This variable has been set constant in the present numerical simulations, and thus the potential effects related to its variability have not been considered. As this property is both accessible form an experimental point of view and useful as a predictor of the suspension stability (an aspect particularly relevant in the liquid-fine solid phase system), it would be interesting to include a transport model for it.

Acknowledgements

The authors gratefully acknowledge support from the Department of Mining Engineering of University of Chile and the Chilean National Commission for Science and Technology through Fondecyt Project 1160971 and Project INNOVA CORFO Project CSIRO Chile 10CEII-9007.

References

Abu-Jdayil, B., 2011. Rheology of sodium and calcium bentonite-water dispersions: effect of electrolytes and aging time. Int. J. Miner. Process. 98 (3), 208–213.
Abulnaga, B.E., 2002. Slurry Systems Handbook. McGraw-Hill, New York.
Al-Qunaibit, M.H., Mekhemer, W.K., Zaghloul, A.A., 2005. The adsorption of Cu (II) ions on bentonite–a kinetic study. J. Colloid Interface Sci. 283 (2), 316–321.
Atesok, G., Somasundaran, P., Morgan, L.J., 1988. Adsorption properties of Ca^{2+} on Na-kaolinite and its effect on flocculation using polyacrylamides. Colloids Surf. 32, 127–138.
Au, P.-I., Leong, Y.-K., 2013. Rheological and zeta potential behaviour of kaolin and bentonite composite slurries. Colloids Surf. A: Physicochem. Eng. Aspects 436, 530–541.
Bethke, C.M., 2007. Geochemical and Biogeochemical Reaction Modeling. Cambridge University Press.
Boger, D.V., 2009. Rheology and the resource industries. Chem. Eng. Sci. 64 (22), 4525–4536.
Bulatovic, S.M., 2007. Handbook of Flotation Reagents: Chemistry, Theory and Practice: Volume 1: Flotation of Sulfide Ores. Elsevier.
Carroll, D., Starkey, H.C., 1958. Effect of sea-water on clay minerals. In: Clay and Clay Minerals, Proceedings of the 7th National Conference of Clays and Clay Minerals.
Colwell, J.M., Shook, C.A., 1988. The entry length for slurries in horizontal pipeline flow. Canad. J. Chem. Eng. 66 (5), 714–720.
Concha, F., 2014. Solid-Liquid Separation in the Mining Industry. Springer.
Ekambara, K., Sanders, R.S., Nandakumar, K., Masliyah, J.H., 2009. Hydrodynamic simulation of horizontal slurry pipeline flow using ANSYS-CFX. Indus. Eng. Chem. Res. 48 (17), 8159–8171.
Enwald, H., Peirano, E., Almstedt, A.-E., 1996. Eulerian two-phase flow theory applied to fluidization. Int. J. Multiphase Flow 22, 21–66.
Farrokhpay, S., Bradshaw, D.J., 2012. Effect of clay minerals on froth stability in mineral flotation: a review. In: 26th International Mineral Processing Congress, IMPC 2012: Innovative Processing for Sustainable Growth-Conference Proceedings, Technowrites, pp. 4601–4611.
Gillies, R.G., Shook, C.A., Xu, J., 2004. Modelling heterogeneous slurry flows at high velocities. Canad. J. Chem. Eng. 82 (5), 1060–1065.
Grim, R.E., 1968. Clay Mineralogy.
Jacobs, B.E.A., 2003. Design of Slurry Transport Systems. CRC Press.
Karnland, O., Birgersson, M., Hedström, M., 2011. Selectivity coefficient for Ca/Na ion exchange in highly compacted bentonite. Phys. Chem. Earth, Parts A/B/C 36 (17), 1554–1558.
Kaushal, D.R., Sato, K., Toyota, T., Funatsu, K., Tomita, Y., 2005. Effect of particle size distribution on pressure drop and concentration profile in pipeline flow of highly concentrated slurry. Int. J. Multiphase Flow 31 (7), 809–823.
Kraepiel, A.M.L., Keller, K., Morel, F.M.M., 1999. A model for metal adsorption on montmorillonite. J. Colloid Interface Sci. 210 (1), 43–54.
Ndlovu, B., Becker, M., Forbes, E., Deglon, D., Franzidis, J.-P., 2011. The influence of phyllosilicate mineralogy on the rheology of mineral slurries. Miner. Eng. 24 (12), 1314–1322.
Ndlovu, B., Farrokhpay, S., Bradshaw, D., 2013. The effect of phyllosilicate minerals on mineral processing industry. Int. J. Miner. Process. 125, 149–156.
Nguyen, Q.D., Boger, D.V., 1998. Application of rheology to solving tailings disposal problems. Int. J. Miner. Process. 54 (3–4), 217–233.
Peng, Y., Zhao, S., 2011. The effect of surface oxidation of copper sulfide minerals on clay slime coating in flotation. Miner. Eng. 24 (15), 1687–1693.
Poloski, A.P., Etchells, A.W., Chun, J., Adkins, H.E., Casella, A.M., Minette, M.J., Yokuda, S.T., 2010. A pipeline transport correlation for slurries with small but dense particles. Canad. J. Chem. Eng. 88 (2), 182–189.
Rhodes, M.J., Ebrary, I., 2008. Introduction to Particle Technology, vol. 311 Wiley Online Library.
Richardson, J.F., Zaki, W.N., 1954. Sedimentation and fluidisation; part 1. Trans. Inst. Chem. Eng. 32, 35–53.
Rusche, H., 2003. Computational Fluid Dynamics of Dispersed Two-Phase Flows At High Phase Fractions. PhD Thesis. Imperial College London (University of London).
Sato, Y., Sekoguchi, K., 1975. Liquid velocity distribution in two-phase bubble flow. Int. J. Multiphase Flow 2 (1), 79–95.
Schulte, B., Konopliv, N., Meiburg, E., 2016. Clear salt water above sediment-laden fresh water: interfacial instabilities. Phys. Rev. Fluids 1 (1), 12301.
Shook, C.A., Roco, M.C., 2015. Slurry Flow: Principles and Practice. Elsevier.
Speziale, C.G., 1982. On turbulent secondary flows in pipes of noncircular cross-section. Int. J. Eng. Sci. 20 (7), 863–872.
Svarovsky, L., 2000. Solid-Liquid Separation. Butterworth-Heinemann.
Tang, L., Sparks, D.L., 1993. Cation-exchange kinetics on montmorillonite using pressure-jump relaxation. Soil Sci. Soc. Am. J. 57 (1), 42–46.
Tarchitzky, J., Chen, Y., Banin, A.S., 1993. Humic substances and pH effects on sodium- and calcium-montmorillonite flocculation and dispersion. Soil Sci. Soc. Am. J. 57 (2), 367–372.
Taylor, A., Whitelaw, J., Yianneskis, M., 1982. Curved ducts with strong secondary motion: velocity measurements of developing laminar and turbulent flow. J. Fluids Eng. 104 (3), 350–359.
Versteeg, H.K., Malalasekera, W., 2007. An Introduction to Computational Fluid Dynamics: The Finite Volume Method. Pearson Education.
Voegelin, A., Vulava, V.M., Kuhnen, F., Kretzschmar, R., 2000. Multicomponent transport of major cations predicted from binary adsorption experiments. J. Contam. Hydrol. 46 (3), 319–338.
Wilson, K.C., Addie, G.R., Sellgren, A., Clift, R., 2006. Slurry Transport Using Centrifugal Pumps. Springer Science & Business Media.
Zarzycki, P., Szabelski, P., Piasecki, W., 2007. Modelling of ζ-potential of the montmorillonite/electrolyte solution interface. Appl. Surf. Sci. 253 (13), 5791–5796.
Zhang, M., Peng, Y., 2015. Effect of clay minerals on pulp rheology and the flotation of copper and gold minerals. Miner. Eng. 70, 8–13.
Zhou, Z., Scales, P.J., Boger, D.V., 2001. Chemical and physical control of the rheology of concentrated metal oxide suspensions. Chem. Eng. Sci. 56 (9), 2901–2920.